DTT hybrid scenario development with ASTRA-TGLF predictive modelling

J. Lombardo[1,2], F. Auriemma[1,3], A. Castaldo[4], T. Luda[5], P. Mantica[6], G. Rubino[7], B. Baiocchi[6], L. Figini[6], R. Lorenzini[1,4]

1. Consorzio RFX (CNR, ENEA, INFN, University of Padova, Acciaierie Venete SpA), C.so Stati Uniti 4, 35127 Padova, Italy 2. CRF - University of Padova, Italy 3. ISTP, CNR, Padova, Italy 4. ENEA C.R. Frascati, Frascati, Italy 5. Max Planck Institute for Plasma Physics, Boltzmannstr. 2, 85748 Garching, Germany 6. ISTP, CNR, Milano, Italy 7. ISTP, CNR, Bari, Italy

The hybrid scenario and DTT facility

The hybrid scenario represents an operational regime in tokamak devices characterised by improved confinement and stability properties compared to the baseline scenario. It typically features a flat core safety factor profile (q), with $q(\rho = 0) > 1$ and reduced MHD activity. The Divertor Tokamak Test (DTT) facility, which is currently under construction at the ENEA Research Center in Frascati (Italy), has the main objective of developing and testing alternative power exhaust solutions to bridge the gap between ITER and DEMO in reactor-relevant operating regimes[1], among these, the hybrid scenario. The full-power hybrid scenario E developed for DTT operates with the following flat-top parameters: plasma current $I_p = 3.8\ MA$, toroidal magnetic field $B_t = 5.85\ T$, and a total auxiliary heating power of approximately $45 \sim MW$. The heating mix consists of 32 MW of Electron Cyclotron Resonance Heating (ECRH), 6 MW of Ion Cyclotron Resonance Heating (ICRH), and 10 MW of Neutral Beam Injection (NBI)[2].

The ASTRA code and equilibrium

The development of the DTT hybrid scenario E was carried out using a time-dependent analysis with the ASTRA transport code[3]. ASTRA was coupled with TGLF-SAT2, NCLASS, and FACIT, following the same framework adopted for the DTT baseline scenario[2] evolving self-consistenly the electron density (n_e), impurity densities (n_{imps}), electron temperature (T_e), ion temperature (T_i), and plasma current density (j_p) during the ramp-up (RU), flat-top (FT) and ramp-down (RD) phases. The ramp-down is not reported in this work, but it is still under development. The plasma boundary was computed by the CREATE-NL code, ensuring compatibility with the DTT superconducting magnetic systems. Inside the last closed flux surface (LCFS), plasma equilibrium was computed self-consistently using the SPIDER module integrated within ASTRA. The development of the scenario was carried out in synergy with the METIS code[4]. During the RU phase, the line-averaged electron density is feedback-controlled at 30% of the Greenwald limit, and increased to 45% during the FT. The edge boundary condition for T_e is set using the two-point model, whereas the T_i is fixed by imposing the ratio $T_i(\rho = 1)/T_e(\rho = 1)$ at 1.1 and $n_e(\rho = 1)$ at 40% of the target line-averaged density. The edge impurity density $n_{imp1}(\rho = 1)$ is prescribed to maintain $P_{rad} = 0.25 \cdot P_{sep}$ and the ratio

n_{imp2}/n_{imp1} is set at 0.15. The evolution of impurity profiles is computed self-consistently using the FACIT module for the neoclassical transport and TGLF for the turbulent transport.

Current Ramp-Up

An ohmic RU with a current overshoot (OS), similar to that adopted in JET [5], was tested to flatten the q-profile. Although this approach proved effective in reducing magnetic shear, it is not suitable for DTT operations. Due to the high plasma resistivity and limited current RU rate, current diffusion is too rapid, resulting in $q < 1$ already at the beginning of the FT phase, thus negating the potential benefits of the OS. Consequently, controlling the current profile can only be effectively achieved through electron heating, implemented via ECRH during the RU phase, in order to reduce the plasma resistivity and slow down the current diffusion. Several tests were conducted to investigate the optimal deposition profile of ECRH for shaping the q-profile. Additionally, the impact of co- and counter-current ECCD was assessed. The results show that pure core heating is mainly effective in reducing the current diffusivity. In contrast, the ECCD contributes approximately 10% of the total plasma current during the RU phase and has a limited effect on the q-profile; for this reason, it is not applied at this stage of development.

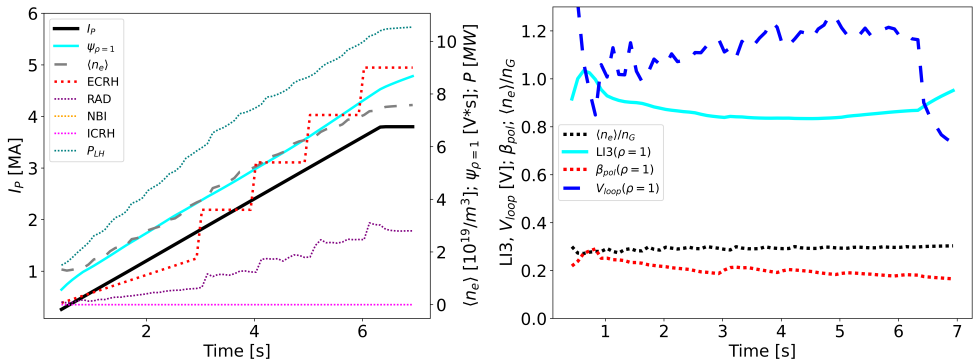

Fig. 1 In the left panel, the plasma current (I_p) is shown as a solid black line, the magnetic flux consumption (ψ_p) as a solid cyan line, and the line-averaged density as a dashed grey line. The injected EC power is represented by a red dotted line, while the radiated power (P_{rad}) is shown as a dotted purple line. In the right panel, the Greenwald fraction is reported in a dotted black line. The $LI3$, β_{pol} and v_{loop} are represented by the solid cyan line, dotted red line, and dashed blue line, respectively.

Given these results, the selected approach is to avoid the OS and assist with EC from the start of the RU. Figure 1 summarises the key features of the RU phase. In the left panel, the plasma current (I_p) and the line-averaged density ($< n_e >$) are reported. The magnetic flux consumption (ψ_p) is kept below $10\ V \cdot s$, preserving solenoid flux and allowing for a sufficiently long discharge. During the limiter phase (0.33–3 s), a pair of gyrotrons (1.8 MW) is activated with a ramp to limit current diffusion, which is particularly strong in the early phase of the discharge. After 3 s, in the divertor configuration, additional gyrotrons are gradually switched on, reaching a total of 9 MW of ECRH power at the start of the FT. The injected power during RU is limited to remain below the L–H threshold (P_{LH}), ensuring that H-mode ($P_{sep} > P_{LH}$) is only accessed at the beginning of the FT. The ICRH and NBI systems are switched off during

the RU phase. In the right panel, the ratio of the $\langle n_e \rangle$ to the Greenwald density is fixed at 0.3. The value of the internal inductance $LI3$ is kept below 1.0, β_{pol} is about 0.2, and the v_{loop} is less than 1.2 V during the whole RU.

Flat-Top

At the beginning of the FT phase, the full auxiliary heating power is injected to trigger the L–H transition. Figure 2 shows the heating configuration chosen for the hybrid scenario, where ECRH reaches 28.8 MW at $t = 7$ s, while ICRH delivers about 6 MW, and NBI injects 10 MW at 510 keV. Power deposition profiles are modelled in ASTRA using Gaussian functions for ECRH and ICRH, and the RABBIT code for NBI. Intense oscillations in the density trace are observed at the L–H transition, likely due to feedback instability in gas puff control, indicating the need for further tuning of the density regulation system.

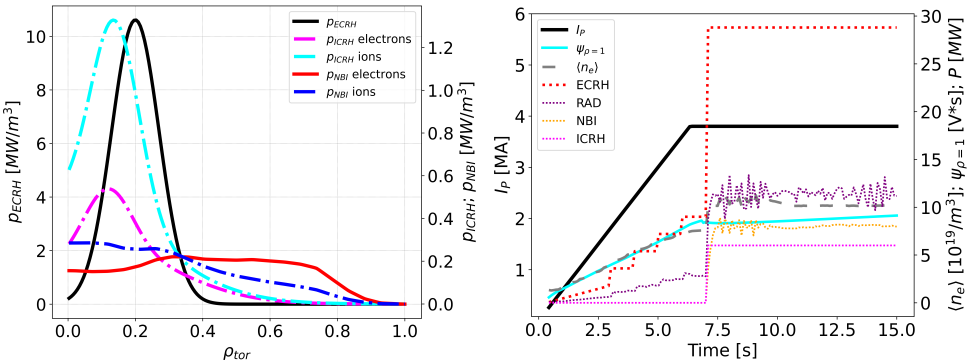

Fig. 2 In the left panel, the profiles of deposition are shown: ECRH, ICRH (on electrons and ions) and NBI (on electrons and ions) are represented by the black, pink, cyan, red and blue lines, respectively. In the right panel, the plasma current (I_p) is shown as a solid black line, the magnetic flux consumption (ψ_p) as a solid cyan line, and the line-averaged density as a dashed grey line. Red, pink and yellow dotted lines, respectively, represent the injected EC, IC and NBI power. The radiated power (P_{rad}) is shown as a dotted purple line.

Upon entering H-mode, the evolution of the kinetic profiles is computed in the core region ($\rho \in [0, 0.9]$), while in the edge region ($\rho \in [0.9, 1]$), the profiles are fixed using pedestal models. In this work, the H-mode pedestals are prescribed using analytical expressions, with the same pedestal widths and the same ratio between L-mode and H-mode pedestal heights as those obtained in the DTT scenario E baseline configuration, computed with the IMEP code. A self-consistent pedestal prediction is currently being developed using the stand-alone version of the IMEP code for the hybrid scenario as well. For the hybrid scenario, preliminary results indicate that the pedestal pressure computed with IMEP is consistent with the values obtained from the analytical model, confirming that the choice of the analytical approach for the pedestal is close to the actual profiles. The main results obtained during the FT phase are shown in Figure 3, which shows the evolution of the radial profiles of T_e, T_i, n_e, q and impurities. The L-mode profiles are shown with black solid lines, and the H-mode profiles with red solid lines. The q profile remains above 1 throughout most of the discharge, with $q(0) > 1$ maintained at all times, and a local drop of q marginally below one is observed at $\rho \approx 0.15$ for $t > 12$ s.

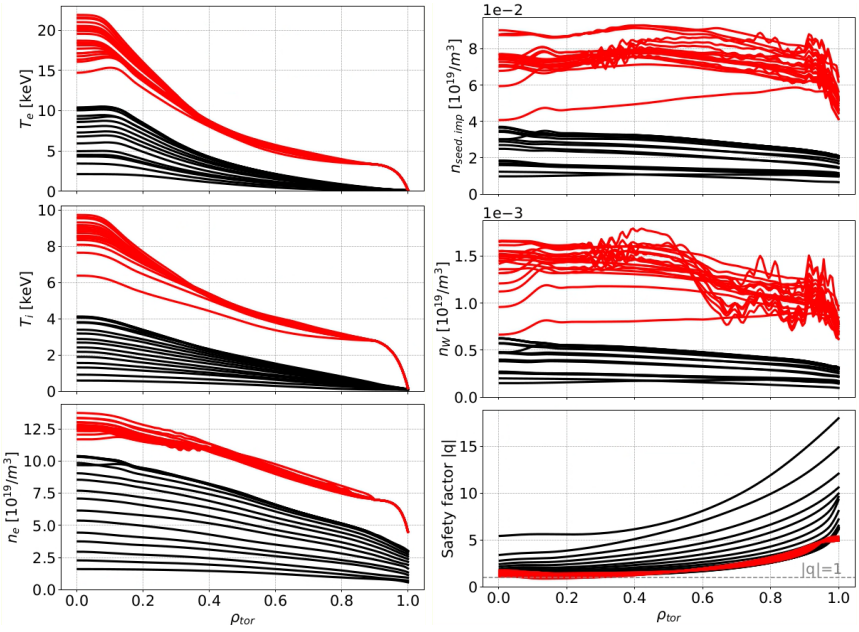

Fig. 3 The evolution of the radial profiles of T_e, T_i, n_e, q and impurities, where the L-mode profiles are shown with black solid lines, and the H-mode profiles with red solid lines.

Conclusions and future works

For the hybrid scenario during the RU and FT phases, the integrated ASTRA-based simulations confirm its feasibility under DTT operational conditions, from both physics and engineering perspectives. The scenario successfully achieves a stationary H-mode with a total heating power of 45 MW. These results demonstrate the potential of the hybrid scenario to operate in reactor-relevant regimes. Future work will focus on several key aspects aimed at further optimising scenario performance. First, the ECRH power deposition during the FT phase will be optimised to broaden the region with a flat q-profile while avoiding local values below 1. A self-consistent computation of pedestal profiles using IMEP code is also underway. Additionally, the power deposition profiles for both ECRH and ICRH will be evaluated using the JINTRAC and GRAY codes to improve localisation and absorption modelling. The possibility of reducing the electron density during the RU phase will also be explored as a means to reduce current diffusion further, and an earlier X-point formation to reduce the tokamak limiter phase is under development. Lastly, the challenges of the ramp-down phase will be addressed to ensure a controlled termination of discharge.

References

[1] F. Crisanti et al. In: Nuclear Fusion 64.10 (2024). DOI: 10.1088/1741-4326/ad6e06.

[2] N. Bonanomi et al. In: Nuclear Fusion 65.1 (2025). DOI: 10.1088/1741-4326/ad8edb.

[3] G. V. Pereverzev et al. 2002.

[4] J. F. Artaud et al. In: Nuclear Fusion 58.10 (2018). DOI: 10.1088/1741-4326/aad5b1.

[5] C. D. Challis et al. In: Nuclear Fusion 55.5 (2015). DOI: 10.1088/0029-5515/55/5/053031.